

V64

Interferometry

Celina Wieberg

celina.wieberg@tu-dortmund.de

Aaron Schink

aaron.schink@tu-dortmund.de

Experiment date: 19.1.2026

Submission date: DATUM

TU Dortmund – Fakultät Physik

Contents

1. Objective	3
2. Theoretical Background	3
2.1. Light and its properties	3
2.1.1. Polarization	3
2.1.2. Coherence	4
2.2. Interferometry	4
2.3. Index of refraction	5
2.3.1. Refractive index of glass	6
2.3.2. Refractive index of air	6
3. Setup and Experiment	7
3.1. Sagnac interferometer	7
3.2. HeNe-Laser	7
3.3. PBSC	8
3.4. Experiment	9
3.4.1. Alignment	9
3.4.2. Contrast	9
3.4.3. Refractive index of glass	9
3.4.4. Refractive index of air	9
4. Analysis	10
4.1. Contrast	10
4.2. Refractive index of glass	11
4.3. Refractive index of air	11
5. Discussion	13
5.1. Contrast	13
5.2. Refractive index of glass	13
5.3. Refractive index of air	13
A. Original Data	15
References	19

1. Objective

In this experiment, the contrast of a Sagnac interferometer is measured, as well as the index of refraction of glass and gases.

2. Theoretical Background

In this section, the theoretical background for interferometry is established. The concepts of polarisation and coherence of light are explained. Equations for intensities, contrasts, angle dependencies and indices of refraction are given.

2.1. Light and its properties

In order to measure interference, the light needs to be coherent and polarized. These two aspects are explained below.

2.1.1. Polarization

Light is an electromagnetic wave, meaning it has two perpendicular oscillating components with respect to its direction of propagation \vec{k} , an electric field \vec{E} and a magnetic field \vec{B} . By convention, the direction polarization is determined by the direction of oscillation of the electric wave component [2]. Usually, light from most sources is **unpolarized** or rather **randomly polarized**, meaning the direction of oscillation of the electric field changes rapidly. Using a polarizing effect, it is possible to extract a preferred mode of oscillation. These effects can be found in birefringent polarizers like calcite, reflection polarizers using the Brewster's angle, or dichroistic absorbers like polyvinyl alcohol [3]. The light is then **linearly polarized**, meaning the electric field only oscillates in one direction. If two linearly polarized beams are superimposed perpendicular to one another with the same magnitude in their respective \vec{E} and a phase difference of $|\frac{\pi}{2}|$, the result is **circularly polarized** light where the sum of the electric field vectors follows a circle. Depending on the phase of the linearly polarized waves, one differentiates between right circular and left circular polarization. Lastly, if the superimposed waves do not have the same magnitude, the resulting light has **elliptical polarization**. Linear, circular and elliptical polarization are shown in Figure 1.

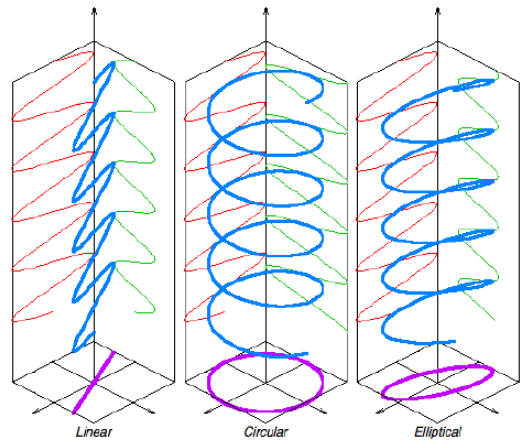


Figure 1: Three possible polarizations of light. The superimposed waves are shown in red and green in the back, the resulting wave in blue in the middle of each example. On the bottom, the path of the resulting field vector is shown [1].

2.1.2. Coherence

Coherence describes the correlation of points in a wave at different points in space or time. For this purpose, one differentiates between **temporal coherence** and **spatial coherence**. A temporally coherent wave has a set phase relation at one point in space at different points in time. This means it is possible to predict the phase of a wave for all times t , i. e., it has a fixed period T . This is only true for ideally monochromatic light that has only one wavelength λ or frequency ν . Real sources, however, emit in a small spectrum causing the frequency of around $1 \cdot 10^{15}$ Hz to fluctuate slowly. The time in which it is possible to predict the phase is called the **coherence time** Δt_c for which it holds that

$$\Delta t_c = \frac{1}{\Delta\nu}$$

with the spectral width $\Delta\nu$ [4].

Analogously, spatial coherence describes the correlation of different points in space at one point in time. It has a fixed wavelength λ or wavenumber k . Sometimes, the concept of spatial coherence is applied to light sources: a spatially incoherent light source like a filament light bulb emits light at different point with uncorrelated phases [5].

The degree of coherence is defined as [4]

$$|\tilde{\gamma}_{12}(\tau)| = \left| \frac{\langle E_1(t + \tau) E_2^*(t) \rangle_T}{\sqrt{\langle |E_1|^2 \rangle \langle |E_2|^2 \rangle}} \right| = \gamma \quad (1)$$

with the complex electric fields E_1 and E_2 , the time delay between the two fields τ and the time of observation t . This expression basically quantifies the coherence of two waves. $\gamma = 1$ describes perfect coherence, $\gamma = 0$ complete incoherence. For $0 < \gamma < 1$, waves are partially coherent.

Coherence as well as well as determined polarization are key in lab interferometry experiments.

2.2. Interferometry

Coherent and polarized light is not necessary for interference to take place. E. g., water lipid boundaries are able to produce colorful interference patterns in sunlight, see Figure 2. The reason for this are small path lengths in the film along with the splitting of light in different polarizations according to the Fresnel equations. In lab experiments relying on interference, dimensions are much larger, requiring coherent light with sufficient coherence lengths. The coherence length is related to the previously explained coherence time by

$$\Delta x_c = c \Delta t_c$$

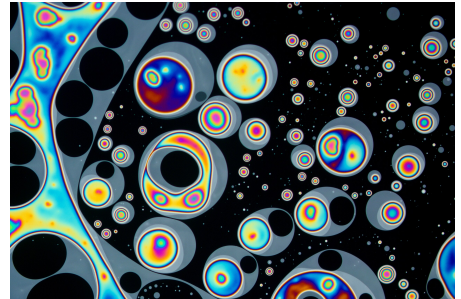


Figure 2: Close up of a water-lipid boundary, showcasing thin-film interference of incoherent, unpolarized light [6].

with the speed of light c . According to the Fresnel-Arago laws [4], two coherent light beams need to have equal linear polarization in order for interference patterns to appear. Lasers produce polarized light in only a few narrow frequencies, meaning they have a large coherence length and are applicable in big experiments. For example, LIGO uses Nd:YAG lasers [7] which ordinarily already have a coherence length of over 1 km [8]. Further stabilization measures are said to increase the coherence length to over $1 \cdot 10^7$ km [7]. Normal lab experiments do not require such immense coherence lengths since the setup is much smaller.

The contrast C or visibility of an interference pattern is defined as

$$C = \left| \frac{I_+ - I_-}{I_+ + I_-} \right| \quad (2)$$

where I_+ and I_- are the maximum and minimum intensity of the fringes, respectively, demonstrated in Figure 3 [5].

Generally, the intensity in an interference pattern created by two equally polarized, coherent beams with intensities I_1 and I_2 is given by

$$I = I_1 + I_2 + 2\sqrt{I_1 I_2} \cos(\delta)$$

with the path difference δ . δ thus determines whether or not there is destructive or constructive interference. It corresponds to the earlier discussed γ in Equation 1 [4]. The maximum intensity I_+ and minimum intensity I_- are then given by

$$I_{\pm} = I_1 + I_2 \pm 2\sqrt{I_1 I_2}. \quad (3)$$

Assuming that a single beam is split under a polarization angle ϕ , i. e., $E_1 = E_0 \cos(\phi)$ and $E_2 = E_0 \sin(\phi)$, it can be shown that Equation 3 simplifies to

$$I_{\pm} \propto I_0(1 \pm \sin(2\phi)), \quad (4)$$

which can be inserted into Equation 2, yielding

$$C = |\sin(2\phi)|. \quad (5)$$

2.3. Index of refraction

The refractive index determines the angle of refraction of light in a medium. Interferometry experiments can be used to determine the index of refraction of different materials like glass or gases. This is generally done by counting the number of interference fringes M . After a phase shift $\delta = 2\pi$, one fringe occurs, meaning

$$M = \frac{\Delta\Phi}{2\pi} \quad (6)$$

2.3.1. Refractive index of glass

If light beams with the vacuum wavelength λ_0 are sent through two glass plates of thickness d rotated by $\Theta_0 = 10^\circ$, they experience phase shifts $\Delta\Phi$ due to the index of refraction. The phase shift in a beam for a given rotation angle Θ of the glass through only one plate at no angle is given as

$$\Delta\Phi(\Theta) \approx \frac{2\pi}{\lambda_0} d \frac{n-1}{2n} (\Theta).$$

A beam that passes through two plates already rotated by Θ_0 experiences a phase shift of

$$\Delta\Phi(\Theta) \approx \frac{2\pi}{\lambda_0} d \frac{n-1}{2n} ((\Theta + \Theta_0)^2 - (\Theta - \Theta_0)^2).$$

The term $(\Theta + \Theta_0)^2 - (\Theta - \Theta_0)^2$ can be expanded, yielding $4\Theta\Theta_0$. Then, using Equation 6, the index of refraction can be written as

$$n = \frac{1}{1 - \frac{M\lambda_0}{2d\Theta\Theta_0}}. \quad (7)$$

According to literature, the index of refraction of glass for a wavelength of 632.99 nm is $n = 1.5151$ [9].

2.3.2. Refractive index of air

If light passes through a gas cell of length L , it undergoes a phase shift given by

$$\Delta\Phi = \frac{2\pi}{\lambda_0} \Delta n L$$

where Δn is the difference of indices of refraction of the investigated media, $\Delta n = n - 1$ for a difference between a medium and the vacuum. Using Equation 6, one can write

$$n = \frac{M\lambda_0}{L} + 1 \quad (8)$$

for the refractive index at different pressures p since M changes with p . The Lorentz-Lorenz law [10] can be approximated for $n \approx 1$ to

$$n = \frac{3}{2} \frac{Ap}{RT} + 1 \quad (9)$$

with the pressure p , molar refraction A , universal gas constant R and the temperature of measurement T . Using Equation 9, the indices of refraction at different pressures can be fitted to obtain n at standard conditions. According to literature, the index of refraction of air for a wavelength of 632.99 nm is $n = 1.000\,276\,53$ [9].

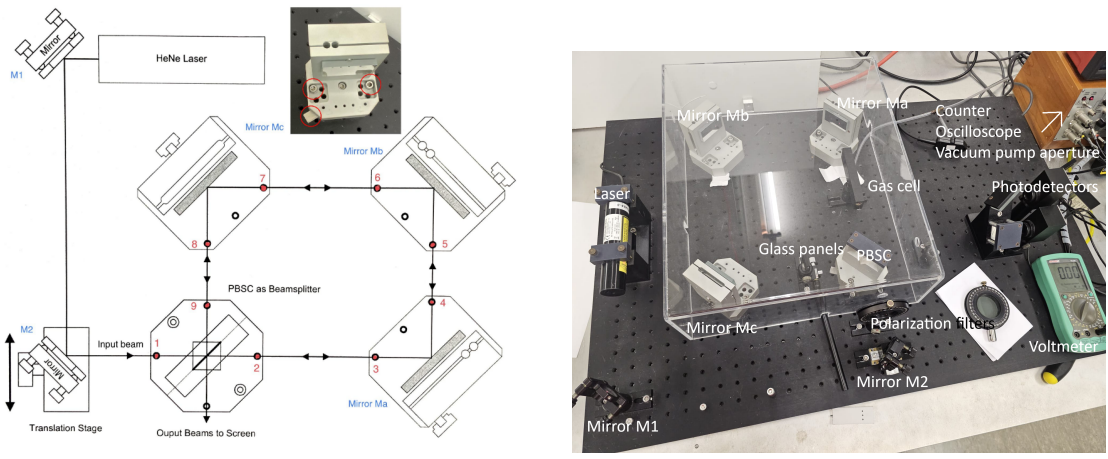
3. Setup and Experiment

The experimental setup and working principles of core components like the laser and polarizer used here are outlined.

3.1. Sagnac interferometer

There are many types of interferometers. A lot of setups require mirrors and beam splitters in order to measure interference. The Michelson interferometer is one of the best known types of interferometers, having been used to disprove the aether theory in 1881 [11] or in LIGO to find gravitational waves in 2016 [12].

In this experiment, a Sagnac interferometer is used, the topology of which is depicted in Figure 4a.



(a) Plan of the Sagnac interferometer used in the experiment.

(b) Realized setup including gas cell, glass panels and polarization filters.

Figure 4: Sketch and realized setup of the Sagnac interferometer used in the experiment.

A Sagnac interferometer works by splitting a coherent polarized beam into two separate beams which follow the same path but in different directions [4]. This causes any disturbance of the positioning of the mirrors, for example, to affect both beams equally, cancelling out, making the interference pattern highly stable against outside disturbances.

3.2. HeNe-Laser

The light source in this experiment is a helium-neon laser. This laser contains a low pressure gas mixture consisting of about 1 part neon and 4 parts helium, the neon being the laser active medium. A laser usually consists of a pump applying a large electric field to excite the medium and a resonator, consisting of two mirrors at either end. One mirror is semi transparent for the light to exit through.

The electric field excites the helium atoms in the container, causing the electrons to gain about 20.61 eV relative to the ground state. Via collisions, this energy is transferred to the neon atoms at about 20.66 eV. These two states are meta stable. Via stimulated emission, the neon emits photons of about 1.96 eV. The excited state of about 18.70 eV is short lived and relaxes under spontaneous emission or collisions with the container. This system is called a 4 level system since four excitation states are involved.

Only the photons emitted by stimulation that are perpendicular to the resonator mirrors are coupled back into the laser, causing more stimulated emission of very coherent, uniformly polarized light. The rest exits the container. The wavelength corresponding to the stimulated photons is about 632.990 nm [13].

Lasers cannot work in 2 level systems because population inversion, i. e., more excited states than ground states, is not possible. Population inversion is important for spontaneous emission to dominate over absorption [14].

3.3. PBSC

A **polarizing beam splitter cube** is a device to split one beam into two perpendicular beams with different but orthogonally linear polarization. It consists of two prisms attached to one another with dielectric layers. An incoming, incoherent, unpolarized light wave hits these media, but only one polarization, namely the one perpendicular to the plane of incidence, causes electrons to oscillate, creating a reflected beam with only one but strong polarization, though weak in intensity, also perpendicular to the plane of incidence. The transmitted beam is strong in intensity but merely partially polarized. With several layers of such dielectric media, it is possible to further split the transmitted beam, increasing the intensity of the reflected beam and further polarizing the transmitted beam [4]. Sketches of the mentioned concepts are depicted in Figure 5.

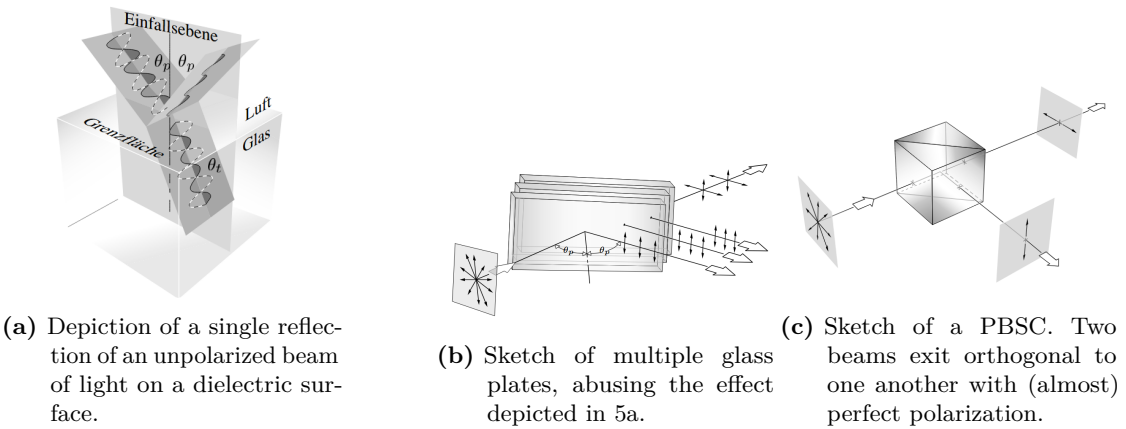


Figure 5: Concepts and sketches of polarization and polarizers [4].

3.4. Experiment

The entire experiment relies on proper alignment which is done before any measurements are taken.

3.4.1. Alignment

The emitted light from the HeNe laser is linearly polarized. The polarization is to be tilted by 45° with respect to the vertical. Using the two mirrors M1 and M2, the beam is coupled into the PBSC and the interferometer by central reflection on the mirrors under 45° each. The beam deflected by the PBSC is blocked and using adjustment plates, the beam passing through the PBSC is centered onto the mirrors Ma and Mc. Then, by adjusting Ma and Mc directly, the beams are centered onto Mb and the PBSC again. Without another polarization filter in front of the detector, no interference pattern can be seen. A filter is inserted to observe the interference pattern on a testing screen. The size and orientation of the fringes can be manipulated by adjusting the mirrors slightly. The interference pattern is to be eliminated by placing the glass plates into the beam and splitting the beams. The mirrors Ma and Mc are adjusted again to create effectively only one big fringe.

3.4.2. Contrast

Using a diode, the contrast of the interference pattern at maximum and minimal intensity can be measured for different angles of polarization Θ . The final polarization filter is removed and the dot on the testing screen or photodetector is set to a maximum intensity. The first polarization filter is rotated in 15° steps from 0° to 180° and the voltage on the photodiode is recorded. This is repeated two more times. Then, the intensity is minimized by adjusting the screws on the mirror and the same measurement is repeated.

3.4.3. Refractive index of glass

Using the double glass holder, the number of interference maxima and minima is measured. Two diodes are used for a differential voltage method, which produces a higher signal to noise ratio. The glass plates have a holder with a rotational element set at 30° . The counter is reset and the rotational element is manually slowly rotated to 40° . The number of maxima and minima is counted. This is repeated several times to ensure good statistics because of instabilities in the setup, causing the interference pattern to shift and the counts to increase rapidly at any slight movements.

3.4.4. Refractive index of air

A gas cell is installed in one of the beams and evacuated. The number of minima and maxima of the interference pattern is measured while the pressure is increased. For this, the ventilation valve is slowly opened. The increase in pressure and counts are recorded with a camera, enabling a simple reading of the data.

4. Analysis

For the analysis, the Python library `numpy` [15] is used. Fits are done using `curve_fit` from `scipy.optimize` [16]. Error analysis is done using `uncertainties` [17]. Plots are created using `matplotlib.pyplot` [18].

4.1. Contrast

The exact measurements for maximum and minimum intensities depending on the angle of polarization are given in Table 1. Due to large fluctuations in the measurement for high voltages, the error of a data point is set at 10 % of the measured voltage. Using Equation 2, the contrast C can be calculated.

Additionally, the angular dependence of the contrast is described by Equation 5. Considering possible sources of errors, one model can be chosen to be

$$C_{\text{model}}(\phi) = C_{\text{off}} + C_0 |\sin(2\phi)|,$$

where C_0 denotes the modulation amplitude of the interferometer and C_{off} accounts for a residual background contrast caused by optical imperfections or slight misalignments in the setup. The results are shown in Figure 6.

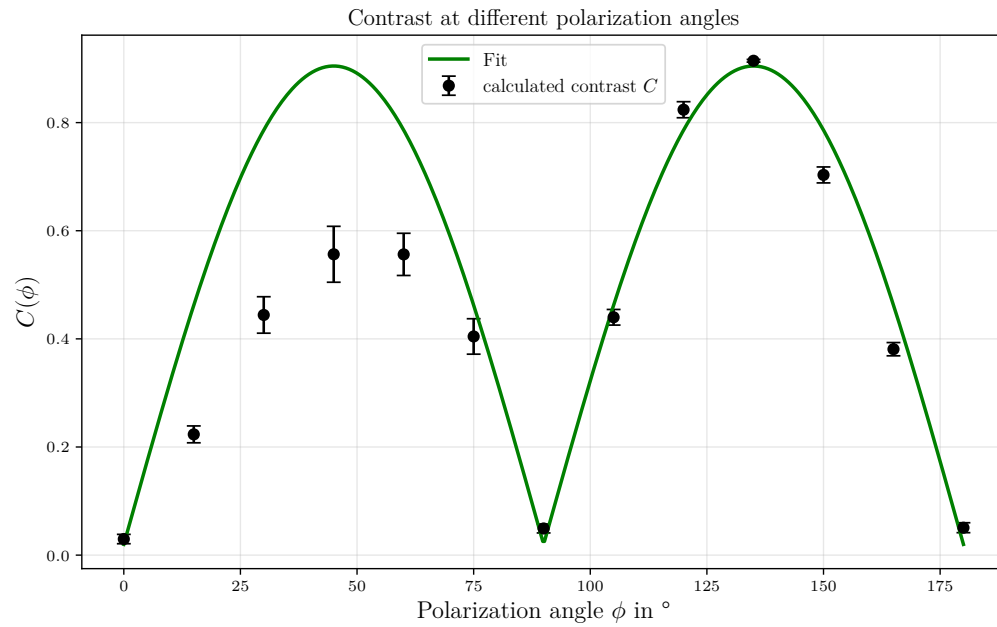


Figure 6: Measured contrast $C(\phi)$ as a function of the polarization angle, together with the fitted model.

The parameters C_0 and C_{off} were obtained from a weighted least-squares fit, where each data point was weighted by $1/\Delta C(\phi_i)^2$. The uncertainties of the fitted parameters correspond to the square roots of the diagonal elements of the covariance matrix.

The fit yields the following parameter values:

$$C_0 = 0.8848 \pm 0.0055,$$

$$C_{\text{off}} = 0.0199 \pm 0.0048.$$

All subsequent measurements in this experiment were performed at a fixed polarization angle of $\phi = 135^\circ$ where the contrast is close to its maximum. This choice ensures a high sensitivity of the interferometer to small phase changes in the following measurements.

4.2. Refractive index of glass

In the experimental configuration, the vacuum wavelength of the laser is

$$\lambda_{\text{vac}} = 632.99 \text{ nm},$$

the initial rotation angle of the glass plates is

$$\Theta_0 = 10^\circ,$$

and the thickness of each glass plate is

$$d = 1 \text{ mm}.$$

Due to the high sensitivity of the counting device, counting uncertainty of two fringes was assumed for M , and the angular precision of the rotation stage was taken as $\Delta\Theta \approx 2^\circ$. Using these uncertainties, the refractive index of glass n was calculated for each measurement using Equation 7,

$$n_{\text{glass}} = 1.4799 \pm 0.1429.$$

The deviation from the literature value of 1.5151 is 2.32 %.

4.3. Refractive index of air

The measurements for the pressure dependent count of fringes as well as the corresponding refractive index differences are listed in Table 2, Table 3 and Table 4 . The cell had a length of $L = (100.0 \pm 0.1) \text{ mm}$. Using Equation 8, the difference in refractive index from vacuum to air can be calculated from the counted number of fringes at a given pressure. The results for all measurements are shown in Figure 7. A linear function

$$\Delta n = m \cdot p + b$$

with m in $1/\text{Pa}$ can be used to fit the data, also shown in Figure 7

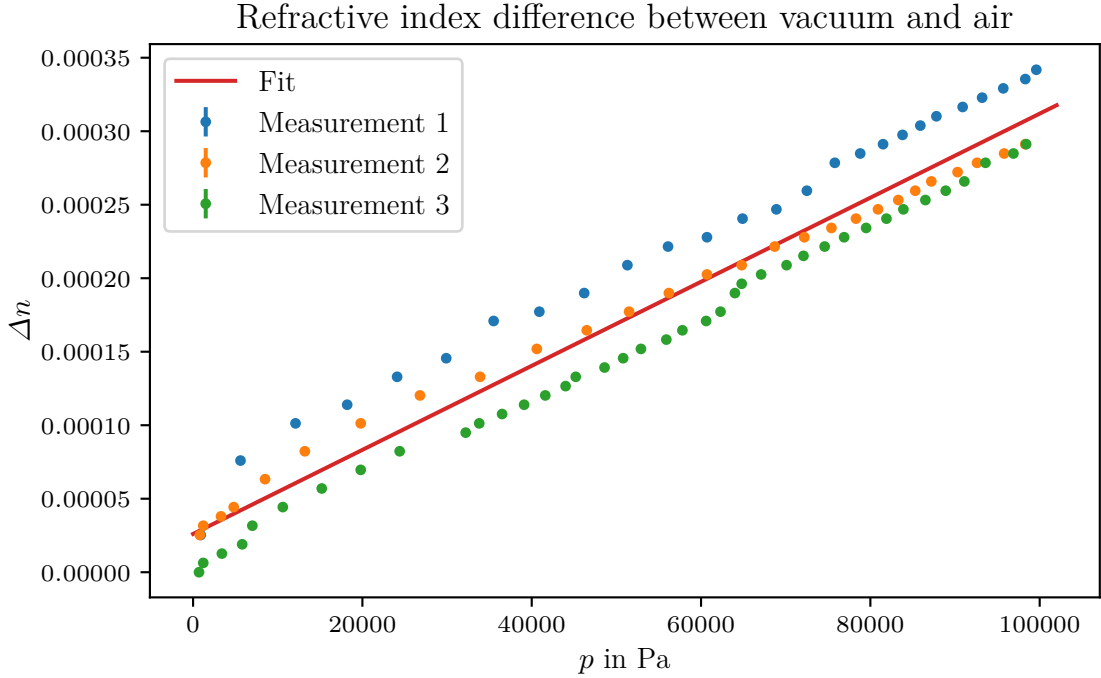


Figure 7: The calculated difference in the refractive index between a vacuum and air of all three measurements, including a linear fit.

The fit parameters are determined to be

$$m = (2.849 \pm 0.078) \cdot 10^{-9} \frac{1}{\text{Pa}}$$

$$b = (2.605 \pm 0.490) \cdot 10^{-5}$$

Using Equation 9 with the universal gas constant $R = 8.3144 \text{ J}/(\text{mol K})$, the molar refractivity of air A for this experiment can be determined from the linear fit,

$$m = \frac{3}{2} \frac{A}{RT}$$

with the previously calculated slope m and the measured room temperature $T = 22^\circ\text{C}$. It follows that

$$A = (4.68 \pm 0.13) \cdot 10^{-6} \frac{\text{m}^3}{\text{mol}}.$$

Inserting this result into the Lorentz-Lorenz law again, the refractive index of air at standard room temperature $T_0 = 15^\circ\text{C}$ and standard room pressure $p_0 = 1013 \text{ hPa}$ can be calculated,

$$n_{\text{air, standard}} = 1.000\,323 \pm 0.000\,009,$$

or more accurately, the difference in refractive index is

$$\Delta n_{\text{air, standard}} = 0.000\,323 \pm 0.000\,009.$$

The deviation from the literature value of 0.000 276 is 17.0 %.

5. Discussion

The interferometric measurements performed in this experiment provide a coherent and mutually consistent picture of the optical properties of the interferometer and the materials placed in its beam paths. By analysing three different aspects of the setup the contrast as a function of the polarization angle, the refractive index of glass, and the pressure dependence of the refractive index of air it is possible to assess both the performance of the interferometer and the reliability of the extracted physical quantities.

5.1. Contrast

The contrast measurement demonstrates that the interferometer operates with high fringe visibility when the polarization angle is chosen appropriately. The fitted modulation amplitude of $C_0 = 0.8848 \pm 0.0055$ indicates that the interferometer is capable of producing nearly ideal interference fringes. The small residual background contrast $C_{\text{off}} = 0.0199 \pm 0.0048$ is physically reasonable and can be attributed to imperfect extinction in the polarizing elements, residual stray light, or slight misalignments in the optical components. The excellent agreement between the measured contrast values and the model $C_{\text{model}}(\phi) = C_{\text{off}} + C_0 |\sin(2\phi)|$ at higher angles confirms that the polarization dependence of the interferometer is well understood. Performing all subsequent measurements at $\phi = 135^\circ$, where the contrast is close to its maximum, is therefore well justified and ensures optimal sensitivity to phase variations. An equally good agreement between theory and experiment should have been measurable for smaller angles. Problems in the proper adjustment of the polarization filter as well as outside factors like unaccounted light sources appeared and may have distorted these measurements slightly.

5.2. Refractive index of glass

The determination of the refractive index of glass yields a value of

$$n_{\text{glass}} = 1.4799 \pm 0.1429.$$

This result is in good agreement with literature values. The relative deviation of approximately 2.32 % is reasonable for a manual interferometric measurement in which the dominant sources of error are the finite angular resolution of the rotation stage and the assumed counting uncertainty of one fringe. Small systematic effects, such as deviations from the nominal plate thickness or slight wedge angles, may also contribute. The biggest factor in deviation is the sensitivity of the counting device, which distorts the measured number of fringes to higher values. Nevertheless, the measured value lies comfortably within the expected range, demonstrating that the interferometer is capable of reliably determining refractive indices of solid materials.

5.3. Refractive index of air

The pressure-dependent measurement of the refractive index of air probes a much smaller effect, since $\Delta n = n - 1$ for air is on the order of 10^{-4} . Despite this, the data exhibit a

clear linear dependence on pressure, as predicted by the ideal gas relation. The linear fit yields

$$m = (2.849 \pm 0.078) \cdot 10^{-9} \frac{1}{\text{Pa}}$$

$$b = (2.605 \pm 0.490) \cdot 10^{-5}$$

from which the molar refractivity is obtained as

$$A = (4.68 \pm 0.13) \cdot 10^{-6} \frac{\text{m}^3}{\text{mol}}.$$

Using the fitted parameters, the refractive index of air at standard atmospheric conditions ($T_0 = 15^\circ\text{C}$, $p_0 = 1013 \text{ hPa}$) is found to be

$$n_{\text{air, standard}} = 1.000\,323 \pm 0.000\,009,$$

which has a relatively large deviation from the literature value at 17.0 %. Since the accuracy of the interferometer has already been demonstrated in previous measurements, the reason for this deviation is most likely in the exceptional sensitivity of the counting device to outside disturbances.

Taken together, the three measurements illustrate both the versatility and the precision of interferometric techniques. The contrast analysis confirms that the interferometer is well aligned and capable of producing high-visibility fringes. The glass measurement shows that refractive indices of solid materials can be determined with percent-level accuracy. The air measurement, in turn, highlights the ability of the interferometer to detect extremely small changes in optical path length, yielding a refractive index in excellent agreement with literature values. The main sources of systematic uncertainty across all measurements are the manual fringe counting, the finite angular resolution of the rotation stage, and possible calibration uncertainties in pressure and temperature. Nevertheless, within the scope of this experiment, the results are highly consistent and demonstrate the reliability of the interferometric approach.

A. Original Data

Angle (°)	I_+ (V)	I_- (V)	I_+ (V)	I_- (V)	I_+ (V)	I_- (V)
0	1.67	1.57	1.72	1.60	1.63	1.56
15	0.94	1.39	0.88	1.40	0.84	1.40
30	0.55	1.27	0.44	1.24	0.43	1.18
45	0.46	1.30	0.37	1.27	0.27	1.29
60	0.55	1.62	0.46	1.62	0.37	1.60
75	0.92	1.86	0.77	1.90	0.71	1.90
90	1.53	1.69	1.57	1.75	1.53	1.67
105	2.58	1.07	2.88	1.08	2.87	1.09
120	3.42	0.40	3.47	0.32	3.67	0.30
135	3.76	0.17	4.04	0.18	4.05	0.18
150	3.81	0.62	3.99	0.75	4.08	0.70
165	2.76	1.26	2.90	1.26	2.95	1.34
180	1.70	1.56	1.79	1.56	1.69	1.56

Table 1: Angle-dependent maximum and minimum voltages from three measurement runs. Due to large fluctuations at higher voltages, the error was set at about 10 % of the measured value.

The number of fringes counted in the measurement for the glass are: 29, 36, 32, 25, 32, 34, 27, 32, 32, 33, 32, 29.

Pressure (mbar)	Counts	$\Delta n(10^{-4})$
9	4	0.2532 ± 0.0003
56	12	0.7596 ± 0.0008
121	16	1.013 ± 0.001
182	18	1.139 ± 0.001
241	21	1.329 ± 0.001
299	23	1.456 ± 0.001
355	27	1.709 ± 0.002
409	28	1.772 ± 0.002
462	30	1.899 ± 0.002
513	33	2.089 ± 0.002
561	35	2.215 ± 0.002
607	36	2.279 ± 0.002
649	38	2.405 ± 0.002
689	39	2.469 ± 0.002
725	41	2.595 ± 0.003
758	44	2.785 ± 0.003
788	45	2.848 ± 0.003
815	46	2.912 ± 0.003
838	47	2.975 ± 0.003
859	48	3.038 ± 0.003
878	49	3.102 ± 0.003
909	50	3.165 ± 0.003
932	51	3.228 ± 0.003
957	52	3.292 ± 0.003
983	53	3.355 ± 0.003
996	54	3.418 ± 0.003

Table 2: Pressure–count measurement (Run 1) at $T = 22^\circ\text{C}$.

Pressure (mbar)	Counts	$\Delta n(10^{-4})$
8	4	0.2532 ± 0.0003
12	5	0.3165 ± 0.0003
33	6	0.3798 ± 0.0004
48	7	0.4431 ± 0.0004
85	10	0.6330 ± 0.0006
132	13	0.8229 ± 0.0008
198	16	1.013 ± 0.001
268	19	1.203 ± 0.001
339	21	1.329 ± 0.001
406	24	1.519 ± 0.002
465	26	1.646 ± 0.002
515	28	1.772 ± 0.002
562	30	1.899 ± 0.002
607	32	2.026 ± 0.002
648	33	2.089 ± 0.002
687	35	2.215 ± 0.002
722	36	2.279 ± 0.002
754	37	2.342 ± 0.002
783	38	2.405 ± 0.002
809	39	2.469 ± 0.002
833	40	2.532 ± 0.003
853	41	2.595 ± 0.003
872	42	2.659 ± 0.003
903	43	2.722 ± 0.003
926	44	2.785 ± 0.003
958	45	2.848 ± 0.003
983	46	2.912 ± 0.003

Table 3: Pressure–count measurement (Run 2) at $T = 22^\circ\text{C}$.

Pressure (mbar)	Counts	$\Delta n(10^{-4})$
7	0	0.000
12	1	0.6330 ± 0.0006
34	2	0.1266 ± 0.0001
58	3	0.1899 ± 0.0002
70	5	0.3165 ± 0.0003
106	7	0.4431 ± 0.0004
152	9	0.5697 ± 0.0006
198	11	0.6963 ± 0.0007
244	13	0.8229 ± 0.0008
322	15	0.9495 ± 0.0009
338	16	1.013 ± 0.001
365	17	1.076 ± 0.001
391	18	1.139 ± 0.001
416	19	1.203 ± 0.001
440	20	1.266 ± 0.001
452	21	1.329 ± 0.001
486	22	1.393 ± 0.001
508	23	1.456 ± 0.001
529	24	1.519 ± 0.002
559	25	1.582 ± 0.002
578	26	1.646 ± 0.002
606	27	1.709 ± 0.002
623	28	1.772 ± 0.002
640	30	1.899 ± 0.002
648	31	1.962 ± 0.002
671	32	2.026 ± 0.002
701	33	2.089 ± 0.002
721	34	2.152 ± 0.002
746	35	2.215 ± 0.002
769	36	2.279 ± 0.002
795	37	2.342 ± 0.002
819	38	2.405 ± 0.002
839	39	2.469 ± 0.002
865	40	2.532 ± 0.003
889	41	2.595 ± 0.003
911	42	2.659 ± 0.003
936	44	2.785 ± 0.003
969	45	2.848 ± 0.003
984	46	2.912 ± 0.003

Table 4: Pressure–count measurement (Run 3) at $T = 22^\circ\text{C}$.

References

- [1] W. Dennis Slafer Vivian K. Walworth. “Generation of circularly polarized stereoscopic transparencies and prints”. In: (2010).
- [2] Edmund Optics. *Introduction to Polarization*. URL: <https://www.edmundoptics.com/knowledge-center/application-notes/optics/introduction-to-polarization/>.
- [3] American Polarizers Inc. *Polarizer – How it Works: Visible Light Linear Polarizers*. URL: [Polarizer%20%E2%80%93%20How%20it%20Works:%20Visible%20Light%20Linear%20Polarizers](https://polarizer%20%E2%80%93%20How%20it%20Works:%20Visible%20Light%20Linear%20Polarizers).
- [4] Eugene Hecht. *Optik*. De Gruyter, 2018.
- [5] A. M. Gretarsson. *A first Course in Laboratory Optics*. Cambridge University Press, 2021.
- [6] Karl Gaff. *Thin-film interference caused by water-lipid boundary*. URL: [https://en.wikipedia.org/wiki/Thin-film_interference#/media/File:Lipid_Islands_on_Soap_Bubble_\(horizontal\).jpg](https://en.wikipedia.org/wiki/Thin-film_interference#/media/File:Lipid_Islands_on_Soap_Bubble_(horizontal).jpg).
- [7] Bas Swinckels. *How are the 4 km arms of LIGO measured so accurately?* URL: <https://physics.stackexchange.com/questions/235865/how-are-the-4-km-arms-of-ligo-measured-so-accurately>.
- [8] COHERENT. *Mephisto MOPA*. URL: <https://www.coherent.com/content/dam/coherent/site/en/resources/datasheet/lasers/mephisto-mopa-ds.pdf>.
- [9] RefractiveIndex.INFO. *Refractive index database*. URL: <https://refractiveindex.info/>.
- [10] S. Selleri G. Pelosi. “Historical corner column: The Clausius-Mossotti and Lorentz-Lorenz relations”. In: (2020).
- [11] TUM. *Michelson-Interferometer (INT)*. TUM. 2021.
- [12] Astrophysik Netzwerk Potsdam. *Gravitationswellen: die Jahrhundert-Entdeckung*. URL: <https://astrophysik-potsdam.de/de/aei-gravitationswellen>.
- [13] TU Dortmund. *V64 Interferometry*. TU Dortmund. 2026.
- [14] LEIFIphysik. *Helium-Neon-Laser*. URL: <https://www.leifiphysik.de/atomphysik/laser/grundwissen/helium-neon-laser>.
- [15] Charles R. Harris et al. “Array programming with NumPy”. In: *Nature* 585.7825 (Sept. 2020), pp. 357–362. DOI: [10.1038/s41586-020-2649-2](https://doi.org/10.1038/s41586-020-2649-2). URL: <https://doi.org/10.1038/s41586-020-2649-2>.
- [16] Pauli Virtanen et al. “SciPy 1.0: Fundamental Algorithms for Scientific Computing in Python”. In: *Nature Methods* 17 (2020), pp. 261–272. DOI: [10.1038/s41592-019-0686-2](https://doi.org/10.1038/s41592-019-0686-2).
- [17] Eric O. Lebigot. *Uncertainties: a Python package for calculations with uncertainties*. Version 3.1.7. URL: <http://pythonhosted.org/uncertainties/>.

- [18] John D. Hunter. “Matplotlib: A 2D Graphics Environment”. Version 1.4.3. In: *Computing in Science & Engineering* 9.3 (2007), pp. 90–95. DOI: 10.1109/MCSE.2007.55. URL: <http://matplotlib.org/>. Current version 3.7.2, DOI: 10.5281/zenodo.8118151.